Journal of Alloys and Compounds 520 (2012) 1–6

Contents lists available at SciVerse ScienceDirect

Journal of Alloys and Compounds

journal homepage: www.elsevier.com/locate/jallcom

Letter

Influence of Yb-doping on the thermoelectric properties of $Pb_{1-x}Yb_xTe$ alloy synthesized using solid-state microwave

A. Hmood*, A. Kadhim, H. Abu Hassan

School of Physics, Universiti Sains Malaysia, 11800 Minden, Penang, Malaysia

ARTICLE INFO

Article history:
Received 24 July 2011
Received in revised form 7 December 2011
Accepted 12 December 2011
Available online 8 January 2012

Keywords:
Thermoelectric materials
Thin films
Microstructure
Electrical transport

ABSTRACT

The semi-magnetic semiconductor thermoelectric alloy $Pb_{1-x}Yb_xTe$ ($0.0 > x < 0.075$) was synthesized by solid-state microwave. Polycrystalline was prepared by high-purity powders for the three elements Pb, Yb, and Te from microwave irradiation-induced equilibrium reaction of initial components to obtain ingots with a large grain size. The morphology of the microstructure and polycrystalline stoichiometric ratio for these ingots was performed using scanning electron microscopy (SEM) and energy dispersive X-ray spectra (EDX). High-quality polycrystalline thin films of $Pb_{1-x}Yb_xTe$ were deposited onto clean glass substrates using the vacuum evaporation technique at 10^{-6} mbar. The structures of the polycrystalline powders and thin films were examined by X-ray diffraction (XRD) patterns. A rock salt structure was observed, and the lattice constant increased with increasing amount of Yb, but not in accordance with Vegard's law. The thermoelectric properties were measured at a temperature range of 298–523 K. Carrier concentrations of the films were determined using Hall effect measurements at 300 K.

1. Introduction

Lead chalcogenide compounds are commonly considered to be promising materials for thermoelectric applications [1]. For mid-temperature power generation (500–900 K), materials based on group-IV telluride are typically used, such as PbTe, $Pb_{1-x}Sn_xTe$, and $AgPb_mSbTe_{2+m}$ [2,3]. The thermoelectric properties of these compounds are highly dependent on the carrier concentration, temperature, and preparation technique [4,5]. Alloys solidified from a stoichiometric melt exhibit a carrier concentration in the order of 10^{17}–10^{18} cm^{-3} at room temperature [6]. Carrier concentration can be changed by doping in some elements as Te, Se, Ag, Cu, In, PbI_2, SbI_3, and Sn. Doping with rare-earth atoms can, in principle, affect transport properties of thermoelectric materials via three mechanisms by the formation of the following: enhanced electron states near the Fermi level, local defects resulting in additional carrier scattering, and additional carrier scattering due to localized magnetic moments [7,8]. Ce, Eu, and Yb rare-earth elements are known to form resonance electron states near the Fermi level and to strongly affect electronic transport properties, particularly thermopower [9] or pseudo binary compounds such as InSb, Bi_2Te_3, Sb_2Te_3, and so on [10,11]. When samples with carrier concentrations higher than 10^{18} cm^{-3} are required, e.g., for thermoelectric energy conversion applications, doping elements are added. Harman [12] has studied low-dimensional structures such as multiple quantum well systems, super-lattices, and quantum dots, which have also attracted much interest in the thermoelectricity field. Another study of low-dimensional effects that require achieving very high crystalline quality and epitaxial growth is generally necessary [13,14]. In that case, thin film deposits have been essentially produced directly onto lattice mismatch substrates such as on the lead salt composition [15]. The present research was initiated to supplement previous works using PbTe-based thin films prepared by multi-techniques such as thermal evaporation [16], sputtering evaporation [17], molecular beam epitaxy [18], plus laser deposition [19], chemical vapor deposition [20], and chemical bath deposition [21]. In the current work, the ternary $Pb_{1-x}Yb_xTe$ alloys were synthesized by exposure to microwave irradiation inside an evacuated silica tube and thermally evaporated to obtain thin films. Finally, their structural and thermoelectric properties were measured.

2. Experimental

$Pb_{1-x}Yb_xTe$ was synthesized as a ternary compound by solid-state microwave standard. Weighted 2 g amounts, according to the stoichiometric ratio $(1-x):x:1$, were prepared from three high-purity element powders (Pb, Te ≥ 99.999% 100 meshes, and Yb ≥ 99.9% 157 μm). The powder was transferred to an agate mortar and pestle and ground for 20 min to obtain a homogeneous mixture. The batched weight was taken in a clean quartz ampoule (10 mm inside diameter × 12 mm outside diameter) and sealed after being evacuated to 10^{-5} mbar. The ampoule was exposed to microwave energy operating at 2.54 GHz with a maximum power of 800 W for about 25 min inside a microwave oven cavity (MS2147C 800 W). This was followed by a working cycle of 5 min exposure and then left to cool down to room temperature. The contents in the ampoule were rocked within a proper

* Corresponding author. Tel.: +60 14 244 1397; fax: +60 46 579 150.
E-mail address: Arshad.phy73@gmail.com (A. Hmood).

0925-8388/$ – see front matter © 2011 Elsevier B.V. All rights reserved.
doi:10.1016/j.jallcom.2011.12.044

Table 1
EDX spectra of $Pb_{1-x}Yb_xTe$ ingots.

x	Element	Weight %	Atomic %
0.0	Te	44.11	56.17
	Pb	55.89	43.83
0.015	Te	42.47	54.46
	Yb	0.66	0.63
	Pb	56.87	44.91
0.03	Te	42.20	54.16
	Yb	1.02	0.97
	Pb	56.78	44.88
0.045	Te	41.78	53.71
	Yb	1.21	1.15
	Pb	57.01	45.14
0.06	Te	42.06	53.99
	Yb	1.33	1.26
	Pb	56.61	44.75
0.075	Te	42.02	53.90
	Yb	1.98	1.87
	Pb	56.00	44.23

redistribution time in-between by interrupting the microwave exposure. This process was repeated for each of the reaction duration. During the reaction time until the end of the formation of the composite, the $Pb_{1-x}Yb_xTe$ compound appeared as a green flash. The morphology and stoichiometric ratio of the microstructure product ingots were examined by SEM & EDX (JSM-6460 LV). The polycrystalline thin films were then deposited onto clean glass substrates by thermal evaporation of 10^{-6} mbar using Alcatel–101. The powders and thin films were measured by XRD (PANalytical X'Pert PRO MRD PW3040). Electrical conductivity and thermoelectric electromotive force (emf) of the films were measured at a temperature range of 298–523 K. The two ends of films were coated with aluminum by thermal evaporation in vacuum using vacuum coater unit Auto 306. The carrier concentration and type of majority carrier were measured by Hall effect using the Vander Paw method at 300 K, which was performed by applying a vertical constant magnetic field of 1 T to the thin films using Lake Shore DEC-603. Film thickness was found to be about 158 ± 6 nm, as measured by Filmetrics F20.

3. Results and discussion

The microwave irradiation technique was used to form PbTe and $Pb_{1-x}Yb_xTe$ compounds, as clearly seen in the SEM images shown in Fig. 1 . The SEM of the PbTe sample reveals the formation of microrods as well as a microstructure. At a higher resolution sequence, a cuboidal tube shape is observed. The morphology of the particles is of closely irregular plates in all cases. Furthermore, the stoichiometric ratio of the microstructure $Pb_{1-x}Yb_xTe$ was used to investigate Yb-doping ratio according to composition analysis (EDX) results (Table 1).

The typical XRD patterns of $Pb_{1-x}Yb_xTe$ ingots synthesized under the same condition by microwave irradiation and thin films are shown in Fig. 2(a) and (b). All the products have a pure-phase present along with rock salt (NaCl)-type structure, confirming the analytical results of the standard database (JCPDS No. 38-1435). The lattice constant of the semi-magnetic semiconductor ternary compound $Pb_{1-x}Yb_xTe$ can be calculated from the XRD data using the cubic system relationship [22]

$$\frac{1}{d^2} = \frac{h^2 + k^2 + l^2}{a^2} \tag{1}$$

Crystallization in the cubic lattice increases with the increase in lattice constant for all doping ingots from $a = 6.4383$ Å to $a = 6.5127$ Å, except for the $x = 0.015$ where there is a decrease to $a = 6.4267$ Å (Fig. 3). This is because for this small fraction of Yb ions ($x = 0.015$) there is a transfer from magnetically active charge state Yb^{3+} ($4f^{13}$) to a non-magnetic Yb^{2+} ($4f^{14}$) charge state which are usually present in $x = 0.03$–0.075 [23,24]. The atomic mass of Yb is 80% compared with the atomic mass of Pb, and the substitution of Yb for Pb induces an increase in the lattice constant a (Å) of the host lattice material PbTe [22]. This increase in the value of lattice constant a was estimated for different composition but not in accordance with Vegard's law; it thus establishes the ytterbium incorporation in the lead telluride lattice, which increases with the increase in partial doping [25]. The lattice constant exhibited in the thin films is similar behavior of powder, as shown in Fig. 3. Similar behaviors have been observed in studies on thin films of a homologous material system $Pb_{1-x}Yb_xTe$ [26], and the increase in lattice constant is not consistent with smaller ion Yb^{+3} (radius 0.91 Å) replacing larger Pb^{+2} (radius 1.2 Å). $Pb_{1-x}Yb_xTe$ is a mixture of the small energy gap (~0.30 eV) PbTe and the wide energy gap (~2 eV) YbTe semiconductors. This substitution induces a continuous change in the nature of the chemical bonding, which is responsible for a linear x-dependence of the lattice constant [27]. This behavior affects the strain of lattice of thin films, which can be calculated by the following equation [28]:

$$\varepsilon_{zz} = \frac{a - a_o}{a_o} \times 100 \tag{2}$$

where a is the lattice constant of the strained $Pb_{1-x}Yb_xTe$ as grown-films, and a_o is the unstrained standard lattice constant of the PbTe compound from JCPDS No. 38-1435. The tensile strain ε_{zz} values increased with increase x fractions, as shown in Fig. 3.

The dc electrical conductivity study is one of the important studies to find the behavior of thin film materials. The electrical conductivity measurement of each composition is carried out at different temperatures varying from 298 to 523 K. The activation energy of the films was also determined using the electrical conductivity data from the Arrhenius relationship [16]

$$\sigma = \sigma_o \exp\left(\frac{\Delta E}{kT}\right) \tag{3}$$

where ΔE is the thermal activation energy of electrical conduction, σ_o is a parameter depending on the semi-conductor nature, and k represents the Boltzmann's constant. Fig. 4 shows the plot of $\ln\sigma$ versus reciprocal temperature the near linear fit of experimental points, indicating the semiconductor nature of all these films. The activation energy value (ΔE) is calculated from two straight lines with different regions for each film so that it has two electronic transitions. The first electronic transition is in the low-temperature region of 300–383 K, whereas the other transition is in the high-temperature region of 443–523 K, indicating that a transition occurred near 383 K (Table 2). Electrical conductivity decreased slightly when the amount of Yb is smaller than 0.03 mol% and then increased slightly at 0.045 mol%. In comparison, at 0.06 and 0.075 mol%, the electrical conductivity dramatically increased at a rate much larger than that of the intrinsic PbTe compound, indicating that the electrical conductivity of $Pb_{1-x}Yb_xTe$ prepared by solid-state microwave is more sensitive to the contents of Yb-doping than that sintered by microwave irradiation. This behavior due to polycrystalline thin films can be explained by the grain boundary trapping according to Baccarani [29]. There are a large number of defects in the grain boundaries because of incomplete atomic bonding [30]. The Yb-doping produces the formation of density of states near the Fermi level; these densities of state oppose and reduce the electrical conduction by capturing the charge carriers at the low-temperature region. At the same time, they increase the mobility of the carriers at high-temperature region (the intrinsic region) due to the reduction of the trapping state and the reduction producing a potential barrier.

Hall effect measurements are performed to estimate the Hall coefficient and carrier concentrations. The results are shown in Table 2. Under the assumption of single-band conduction and a parabolic band model, the carrier concentration at room temperature is obtained from the Hall coefficient using the equation $R_H = 1/ne$, where R_H is the Hall coefficient and n is the carrier concentration. Mobility can be calculated from the carrier

Table 2
The room-temperature Seebeck coefficients ($|S|$), electrical conductivity (σ), Hall coefficients (R_H), carrier concentrations (n), carrier motilities (μ_H), and calculated activation energies (ΔE) at 298 – 523 K of the $Pb_{1-x}Yb_xTe$ thin films.

x	$\lvert S\rvert$ (μV/K)	σ (S/cm)	$S^2\sigma$ (μW/m K^2)	R_H (cm^3/C)	n (cm^{-3})	μ_H (cm^2/V s)	ΔE_1 (eV) (300–383) K	ΔE_2 (eV) (443–523) K
0	102.33	72.315	0.757	−15.7	3.98×10^{17}	1135.345	0.065	0.214
0.015	265	71.413	5.015	−43.98	1.42×10^{17}	3140.743	0.101	0.364
0.03	87	77.167	0.584	−27.04	2.31×10^{17}	2086.595	0.049	0.294
0.045	89	95.79	0.758	−28.9	2.16×10^{17}	2768.331	0.09	0.203
0.06	36	130.752	0.170	−28.7	2.17×10^{17}	3752.582	0.051	0.79
0.075	125.66	97.013	1.532	−42.78	1.46×10^{17}	4150.216	0.094	0.667

concentration and the electrical conductivity according to $\sigma = n \times \mu_H \times e$ (e = electron charge). The carrier concentration of $Pb_{1-x}Yb_xTe$ decreases when the Yb content is increased to 0.03–0.06. Hall mobility increased by increasing the proportion of Yb, except for the decrease at 0.03 and 0.045. These increases in Yb-doping produce high-donor levels near the Fermi level, leading electrons to have light effective mass. An increase in electron density by increasing the doping content of Yb up to 0.075 results

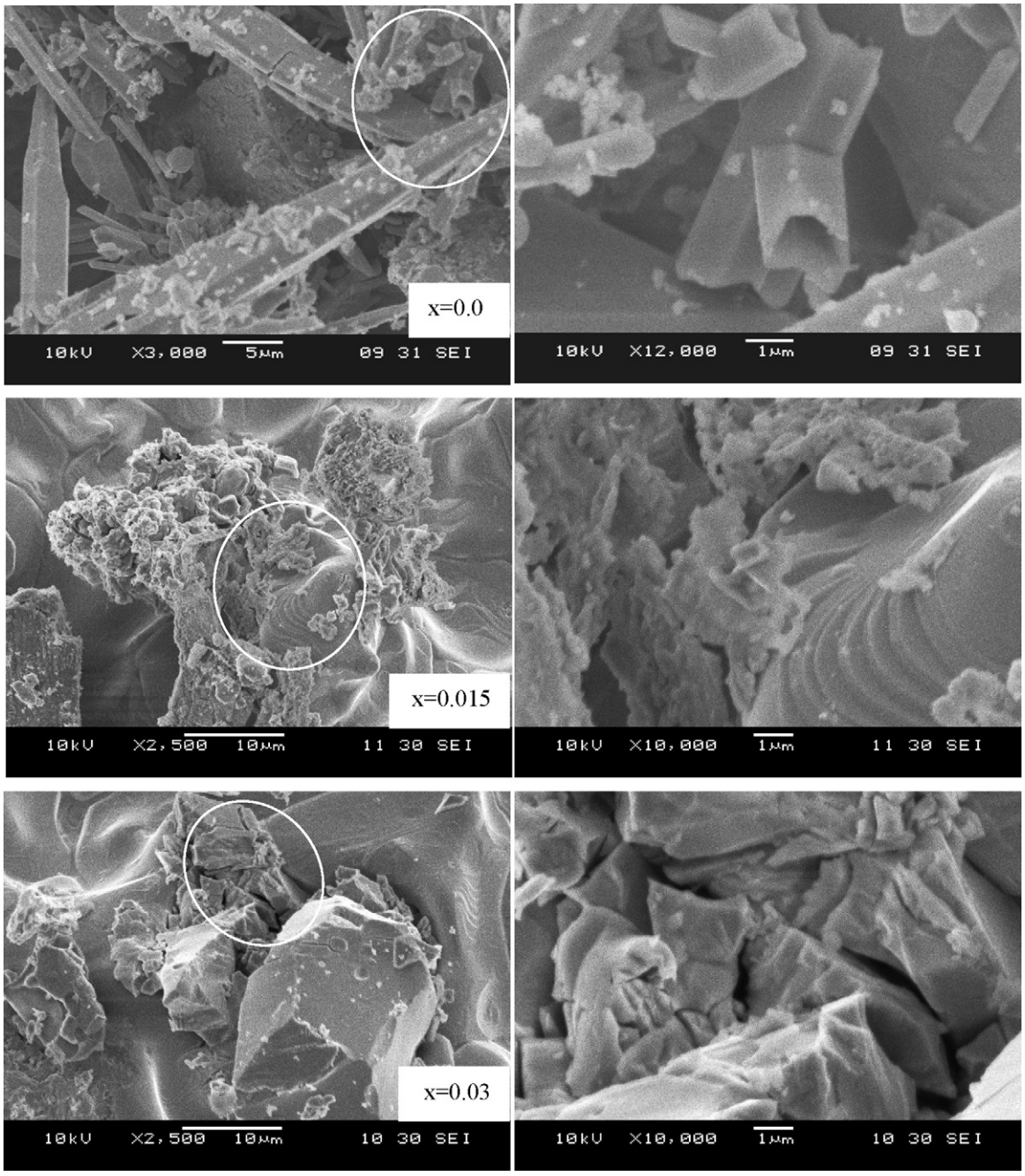

Fig. 1. SEM images of $Pb_{1-x}Yb_xTe$ ingots.

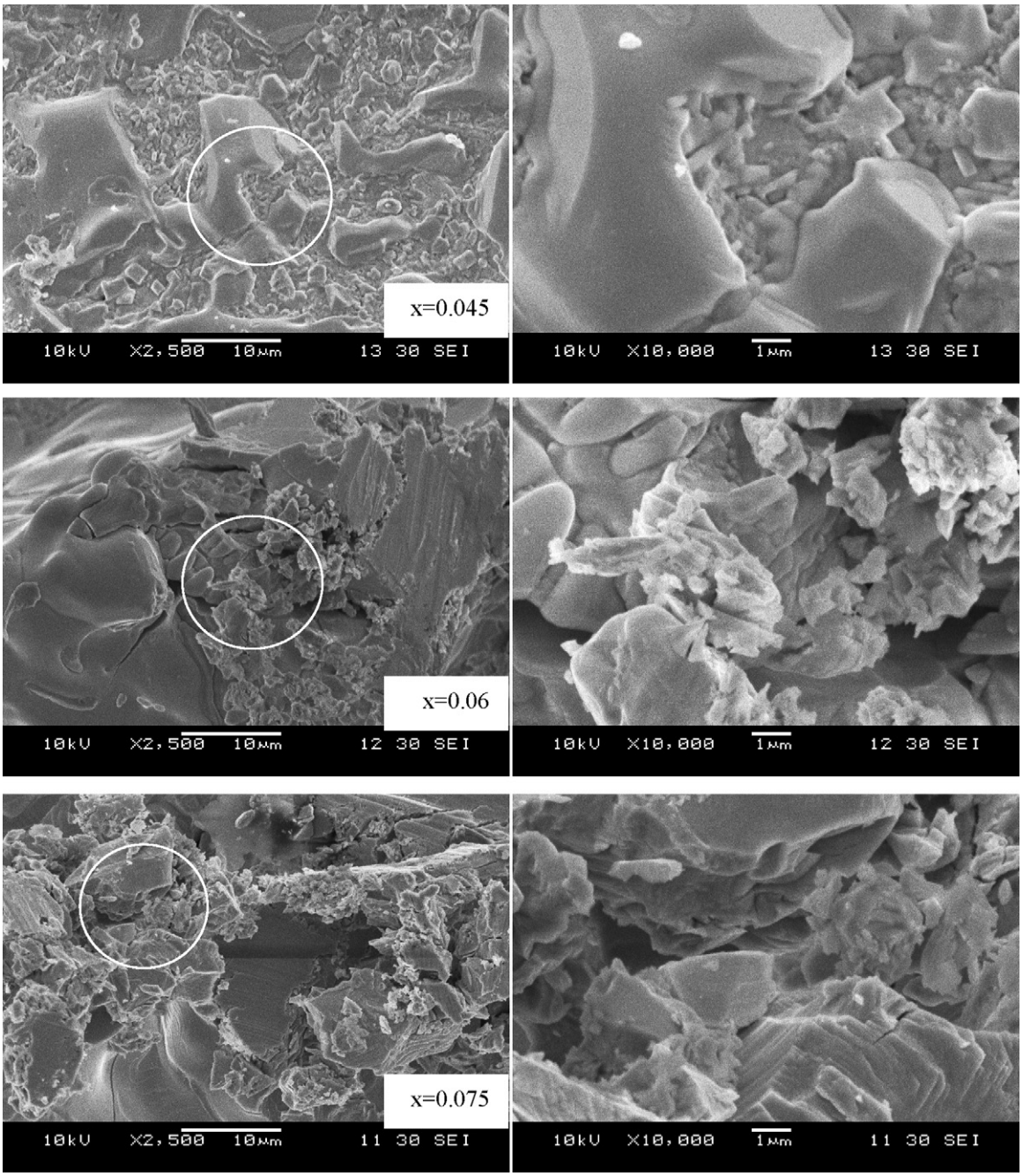

Fig. 1. (*continued*).

in further enhancement of electrical conductivity, primarily due to the escape of majority carrier activation at high temperature.

The thermoelectric power ($S = \Delta V/\Delta T$) determined from the slope of thermoelectric emf versus the temperature difference between the hot and cold ends of the film alloy is shown in Fig. 5. The temperature dependence of the Seebeck coefficient for the Yb-doped films is of semiconductor behaviors, where the values of the Seebeck coefficient increase as the temperature increases. It has similar behavior for all films doped so that the observed sign of the Seebeck coefficient is negative, indicating typical *n*-type semiconductors within the temperature range of 298–523 K; therefore, electrons are the majority carriers in the films. The thermoelectric power of films is found to increase with temperature. A temperature difference causes exciting electrons in the conduction band to diffuse from the hot side to the cold side due to the concentration gradient, causing electric potential and the buildup of charge carriers into the cold side at equilibrium. The Seebeck coefficient for metals or semiconductors under the assumption of parabolic band and energy independent scattering can be expressed as [5]

$$S = \frac{8\pi^2 k^2 T}{3h^2 e} m^* \left(\frac{\pi}{3n}\right)^{2/3} \quad (4)$$

where h is the Planck's constant and m^* is the effective mass of the electron. The above relationship shows that the Seebeck coefficient is highly dependent on the carrier concentration and decreases with increasing carrier concentration. From $x = 0.015$, 0.045, and 0.075 Yb doping concentration, the thermoelectric power of films increases in sequence, whereas at $x = 0.03$ and 0.06, it decreases at

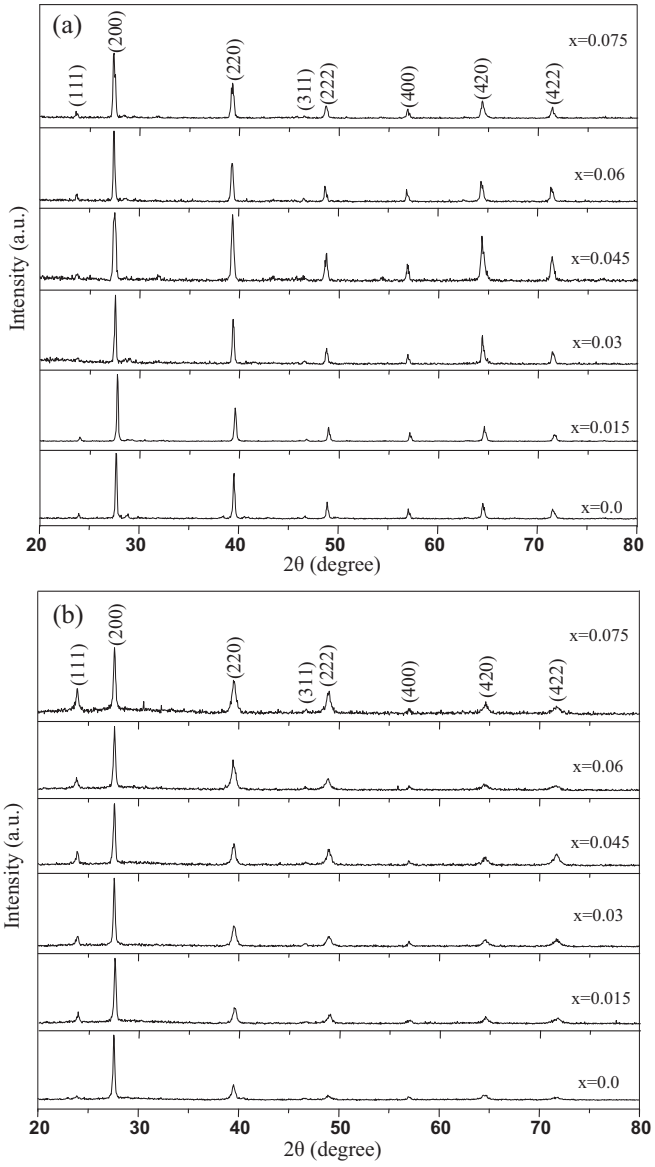

Fig. 2. XRD patterns of $Pb_{1-x}Yb_xTe$ (a) powders and (b) thin films.

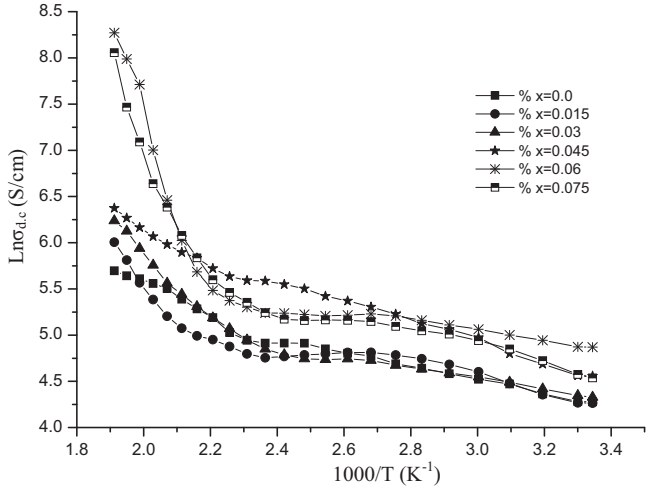

Fig. 4. Plots of various $\ln\sigma$ $1000/T$ of $Pb_{1-x}Yb_xTe$ thin films.

the whole range temperature and then increases at the higher end of the temperature range.

The power factor of the $Pb_{1-x}Yb_xTe$ films $S^2\sigma$ was calculated in terms of the electrical conductivity and Seebeck coefficient, and shown as a function of temperature in Fig. 6. The power factor strongly increases with temperature increase up to 523 K. The value of the power factor is seen to increase dramatically with the increase of the amount Yb-doping. At $x = 0.015$ and 0.075, the highest power factor at room temperature reaches 5.015 and 1.532 $\mu W/m\,K^2$, respectively. Experimental results and theoretical calculations suggest that the electronic transport properties of these films are heavily influenced by a high density of state near the Fermi level leading to a production of electrons with light effective mass [31]. These effective mass carriers lead to a large Seebeck coefficient when $x = 0.015$ and 0.045, while getting high power factors of $x = 0.06$ and 0.075 at 523 K. These results give a clear idea for the application of these alloy compositions for thermoelectric devices. Therefore, these materials have the potential to provide low thermal conductivity and high figure of merit.

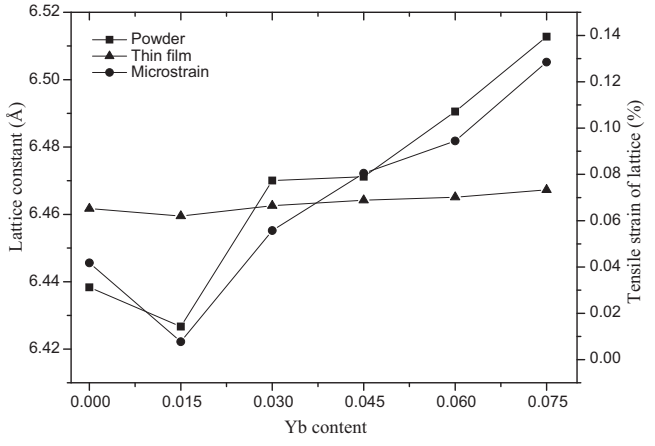

Fig. 3. Variation in lattice constants of polycrystalline powders and thin films of $Pb_{1-x}Yb_xTe$ and variation in tensile strain of thin films with doped Yb content.

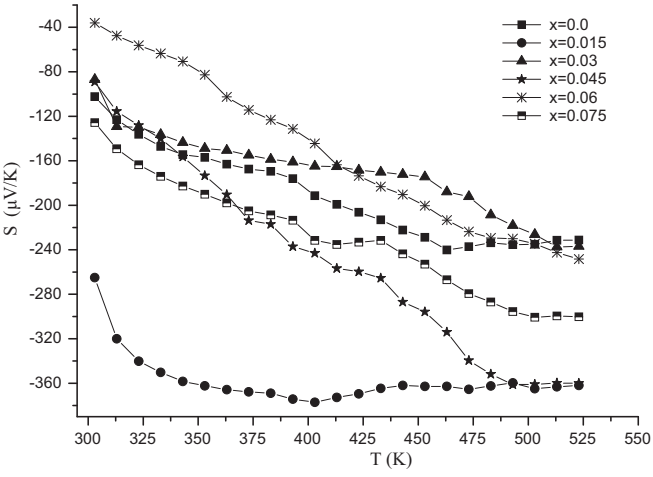

Fig. 5. Temperature dependence of the Seebeck coefficient of $Pb_{1-x}Yb_xTe$ thin films.

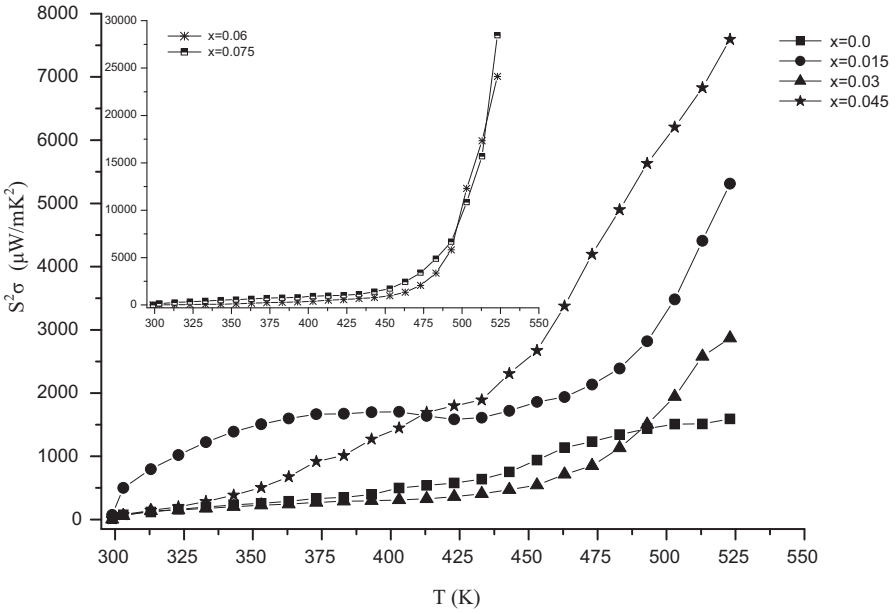

Fig. 6. Temperature dependence of the power factor of $Pb_{1-x}Yb_xTe$ thin films.

4. Conclusions

The present paper reported the polycrystalline synthesis of a cubic NaCl structure for $Pb_{1-x}Yb_xTe$ composition at mole fractions from $x = 0.015$ to 0.075. In addition, the behavior of Yb-doping with increased lattice constant of the powder and thin films was explained. The electrical properties of *n*-type films were measured from ambient temperature up to 523 K. The electrical conductivity increased with the increase in Yb-doping. The Seebeck coefficient increased with the increase of Yb content, except for $x = 0.06$, which was in contrast to both cases. The power factor was maximum at $x = 0.015$, which was 5.015 $\mu W/m\,K^2$ at room temperature, which is promising to produce a high figure of merit.

Acknowledgment

The authors are grateful for the funding provided by the post-graduate research grant scheme (PRGS) (No. 1001/PFIZIK/844134) of Universiti Sains Malaysia.

References

[1] D. Freik, R. Zapukhlyak, M.A. Lopjanka, G.D. Mateik, R.Y. Mikhajlonka, Semicond. Phys.: Quant. Electron. Optoelectron. 2 (1999) 62–65.
[2] S. Qiang, L. Junguo, Z. Lianmeng, Sol. Energy Mater. Sol. Cells 62 (2000) 167–172.
[3] P. David, J. David, Phys. Rev. B 82 (2010), 035204.
[4] P. Joseph, M. Christopher, T. Donald, Phys. Rev. B 70 (2004) 115334.
[5] H.S. Dow, M.W. Oh, B.S. Kim, S.D. Park, B.K. Min, H.W. Lee, D.M. Wee1, J. Appl. Phys. 108 (2010) 113709.
[6] P. Nikoli, W. Konig, D. Lukovi, S. Savi, S. Vujatovi, K. Radulovi, V. Blagojevi, J. Optoelectron. Adv. Mater. 6 (2004) 811–816.
[7] G. Jiangang, J. Xiaopeng, S. Taichao, D. Nan, M. Hongan, J. Alloys Compd. 458 (2008) 428–431.
[8] A. Artamkin, A. Kozhanov, M. Arciszewsk, W. Dobrowolski, T. Story, E. Slynko, V. Slynko, D. Khokhlov, Acta Phys. Pol. A 106 (2004) 223.
[9] I. Radisavljevi, N. Novakovi, N. Romcevi, M. Manasijevi, H-E Mahnkec, N. Ivanovi, J. Alloys Compd. 501 (2010) 159–163.
[10] R. Joseph, J. Robert, K. Huijun, U. Ctirad, G. Mercouri, Chem. Mater. 18 (2006) 4993–4995.
[11] Z. Pinwen, I. Yoshio, I. Yukihiro, S. Yoshikazi, J. Xiaopeng, Z. Guangtian, J. Alloys Compd. 420 (2006) 233–236.
[12] T.C. Harman, D.L. Spears, M.P. Walsh, J. Electron. Mater. 28 (1999) 1.
[13] H. Beyera, J. Nurnusa, H.B. Ottnera, A. Lambrecht, E. Wagnera, G. Bauerb, Physica E 13 (2002) 965–968.
[14] G. Springholz, G. Bauer, G. Ihninger, J. Cryst. Growth 127 (1993) 302–307.
[15] T.C. Harman, D.L. Spears, M.J. Manfra, J. Electron. Mater. 25 (1996) 7.
[16] S. Kumara, B. Lal, S. Rohill, P. Aghamkar, M. Husain, J. Alloys Compd. 505 (2010) 135–139.
[17] R. Wei, C. Wentian, W. Shuyun, S. Mingxiao, L. Huifen, J. Alloys Compd. 509 (2011) 5947–5951.
[18] A. Ueta, G. Springholz, F. Schinagl, G. Marschner, G. Bauer, Thin Solid Films 306 (1997) 320–325.
[19] A. Dauscher, M. Dinescu, O. Boffoue, A. Jacquot, B. Lenoir, Thin Solid Films 497 (2006) 170–176.
[20] D.W. Ma, C. Cheng, J. Alloys Compd. 509 (2011) 6595–6598.
[21] L. Weizhong, W. Xiaofeng, Q. Qiu, W. Fang, L. Zhongkuan, W. Wenjian, J. Alloys Compd. 493 (2010) 358–361.
[22] H.A. Sayadian, H.D. Drew, D.L. Partin, Solid State Commun. 60 (1986) 745–748.
[23] P.M. Nikolic, D. Lukovic, S.S. Vujatovic, K.M. Paraskevopoulos, M.V. Nikolic, V. Blagojevic, T.T. Zorba, B. Stamenovic, W. Konig, J. Alloys Compd. 466 (2008) 319–322.
[24] E.P. Skipetrov, N.A. Chernova, L.A. Skipetrova, E.I. Slynko, Mater. Sci. Eng. B 91–92 (2002) 412–415.
[25] B. Asha, E. Varadarajan, P. Srivastava, H.K. Sehgal, Solid State Commun. 146 (2008) 53–56.
[26] R. Suryanarayan, S.K. Das, J. Appl. Phys. 67 (1990) 1612.
[27] S. Merah, D. Ravot, G.A. Percheron, F.J. Olivier, J.C. Jumas, A. Mauger, E. Parent, J. Alloys Compd. 260 (1997) 17–22.
[28] A.S.H. Hussein, Z. Hassan, S.M. Thahab, S.S. Ng, H. Abu Hassan, C.W. Chin, Appl. Surf. Sci. 257 (2011) 4159–4164.
[29] G. Baccarani, B. Ricco, G. Spadini, J. Appl. Phys. 49 (1978) 5565.
[30] M.M. Ibrahim, E.K. Shokr, S.A. Saleh, E.M.M. Ibrahim, A.M. Abdel Hakeem, J. Non-Cryst. Solids 353 (2007) 2125–2130.
[31] Y. Pei, A.L. Londe, S. Iwanaga, G.J. Snyder, Energy Environ. Sci. 4 (2011) 2085–2089.